The Art of Ceramics
The Blend of Art and Science in Technology
N. Claussen (Editor)

SYMMETRY AND ANTISYMMETRY IN ELECTROCERAMICS

Robert NEWNHAM and Eric CROSS
The Pennsylvania State University, University Park, PA, USA

Many types of symmetry are utilized in ceramic art and in ceramic science. In addition to the common mirror, rotation, inversion and translation symmetry elements observed in crystals and textured ceramics, artists and engineers often make use of the antisymmetry elements involved in color groups. We illustrate the application of color symmetry in controlling the vibration modes in ferroelectric and ferromagnetic ceramics prepared as spheres, hemispheres, and rings conforming to black-and-white Curie groups.

SYMMETRY IN ART AND SCIENCE

While visiting the city of Kütahya, one of the great centers for traditional ceramic tiles and porcelain products, we had the opportunity to view contemporary Turkish artwork. Islamic art has long been famous for its geometric patterns, but we were especially fascinated with the porcelains made by Kervan Chini, who incorporates many interesting symmetries into his pottery. The colorful dish shown in Fig. 1 contains a number of the symmetries and broken symmetries observed in electroceramic materials and devices: polar symmetry, chiral symmetry, symmetry of scale, quasisymmetry, the pseudosymmetry of incommensurate phases, and the antisymmetric elements of color symmetry groups.

Piezoelectric ceramics, pyroelectric glass ceramics, and certain functionally-graded ceramics have polar symmetry like that of a concave-shaped disk (Fig. 2a). Chiral symmetry is present in the porcelain dish as well (Fig. 2b). The leaf pattern of the flowers and the sleeping sheep near the edge are both arranged in a counterclockwise fashion leading to handedness. Chiral phenomena such as optical activity, acoustic activity, and the Faraday Effect are well known in crystal physics. Symmetry of scale is important in all classes of materials. The pattern in Fig. 1 violates the self-similarity principle introduced by Benoit Mandelbrot to describe fractal geometry. Beginning at the center, the porcelain dish shows 5-fold then 9-fold, 10-fold, and 19-fold rotational symmetry. Five-fold symmetry is characteristic of quasicrystals and the circle possesses a ∞-fold axis, one of Curie group symmetries found in textured polycrystalline ceramics. The change in symmetry with scale is illustrated in Fig. 2c.

The symmetry of scale is an important one in many electronic systems as component sizes become smaller and smaller. Current trends in multilayer capacitors are shown in Fig. 3 and 4. The lateral dimensions in MLC chips are now about 1 mm, approaching the limit for many of the pick-and-place machines used in assembling circuits. Layer thicknesses and grain sizes are also a concern. Ceramists are now testing $BaTiO_3$ MLCs with layers of 1 μm thickness which is pressing the limits of tape-casting technology. Particle sizes are in the 0.1 μm range which raises some fundamental questions regarding size effects in ferroelectrics. In large grain size, say 1 μm and larger, each grain contains many domains. The number of domains and the type of domain walls change as grain size drops below a micron. Eventually each grain becomes a single domain with profound changes in dielectric constant and switching behavior. In the nm range the ferroelectric phase transition becomes diffuse and the symmetry of $BaTiO_3$ appears pseudocubic. Size effects in primary ferroics are illustrated schematically in Fig. 5. Dielectric constants drop substantially for grain sizes less than 0.1 μm.

Returning to the porcelain plate in Fig. 1, the outer portions of plate provide an excellent illustration of pseudosymmetry or "almost" symmetry. In the central leaf pattern there are 10 leaves and between neighboring leaves are 10 flowers. Near the outside rim of the plate are red hearts which, at first glance, appear to be in register with the 10 leaves and with the 10 flowers, but such is not in the case. The artist has made a subtle change in symmetry with only 19 hearts instead of 20 (Fig. 2d). Many ferroelectric and ferrimagnetic oxides possess incommensurate structures in which the local polarization or magnetization vectors are out of register with the lattice periodicity (Fig. 6). These so-called incommensurate phases often exhibit unusual physical properties because of their abnormal symmetry.

FERROIC CRYSTALS AND ANTISYMMETRY ELEMENTS

The symmetry elements discussed thus far are purely spatial transformations such as mirror planes, rotation axes, and inversion centers. Spatial symmetry elements are all that are required for the usual crystallographic and limiting point groups, but additional symmetries occur in ferroic electroceramics. These additional symmetries can be described by color symmetry. The ceramic dish from Turkey possesses decagonal color symmetry in which the flower rotates by 36° and changes color (Fig. 2e). In this paper we discuss color groups and the antisymmetry elements found in ferroic ceramics with complex domain patterns. The 10′ antisymmetry element in Fig. 2e belongs to this type of color group.

More than a century ago, the basic relationships between symmetry and physical properties were established by Neumann and the brothers Cu-

rie, and systematized in Woldemar Voigt's monumental "Lehrbuch der Kristallphysik." (Voigt,1928) Using Neumann's Principle, the symmetry restrictions for piezoelectricity, magnetostriction, and other linear and nonlinear tensor properties have been enumerated, and have led to the development of many types of sensors, actuators, and transducers. For single crystals, the properties are governed by the 32 crystallographic point groups, and for textured polycrystalline materials, we use the seven limiting groups first described by Pierre Curie. In 1974 we extended these symmetry arguments to ferroic crystals, laying out the symmetry changes involved in the phase transformations leading to the hysteretic phenomena created by domain wall motion (Newnham, 1974). There are, for example, 15 symmetry changes consistent with pure ferroelastoelectric behavior in which adjacent domains differ only in the orientation of third rank polar tensor properties. A "pure" ferroelastoelectric does not exhibit any other primary or secondary ferroic behavior (Newnham and Cross, 1974).

In crystals with long range magnetic order, the addition of a time reversal operator leads to the generation of the 90 magnetic point groups used to describe ferromagnetic, ferrimagnetic, and antiferromagnetic substances (Birss, 1964). Introduction of the antisymmetric spin reversal operator makes it possible to apply Neumann's Principle to magnetic crystals and classify the symmetry restrictions for magnetic properties such as magnetoelectricity, pyromagnetism and piezomagnetism. All three of these cross-coupled phenomena are axial tensor properties and since spin reversal corresponds to the reversal of an axial vector, all three properties are strongly influenced by the antisymmetry operator.

In this paper we introduce antisymmetry elements for other types of ferroic materials with movable domain walls. Ferroelectricity, ferroelasticity, and the six types of secondary ferroics are also controlled by tensorial antisymmetry operators (Table 1). For a ferroelectric, polarization - a polar vector - is the key operator, since ferroelectricity is defined by polarization reorientation between symmetry related states. For a ferroelastic, the key operator is strain - a second rank polar tensor - since ferroelasticity is defined by strain reorientation between symmetry related states. For a ferrobielastic secondary ferroic, the key operator is a fourth rank tensor, etc.

The procedure will adopt for introducing these antisymmetry elements is as follows. Each operator is combined with the spatial symmetry elements of the 32 crystallographic point groups or to the seven Curie groups to generate a family of antisymmetric groups analogous to the 90 magnetic point groups. Having determined the relevant symmetries, Neumann's Principle is then applied to determine the polar and axial property matrices, enabling one to predict the useful symmetries that will optimize the material for a given

FIGURE 1 - A ceramic dish made by Kervan Chini which illustrates many types of unusual symmetry.

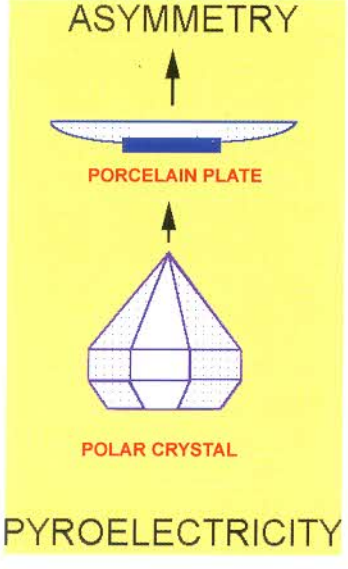

FIGURE 2a - Polarity.

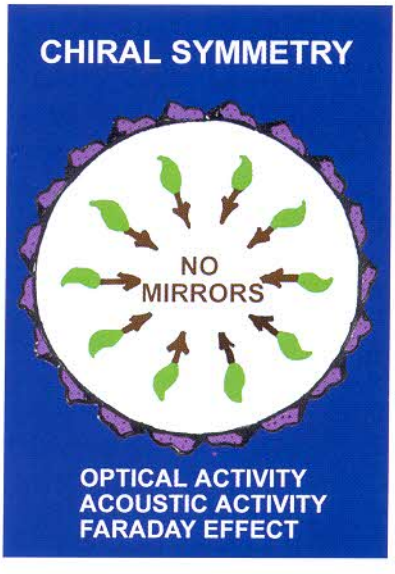

FIGURE 2b - Handedness.

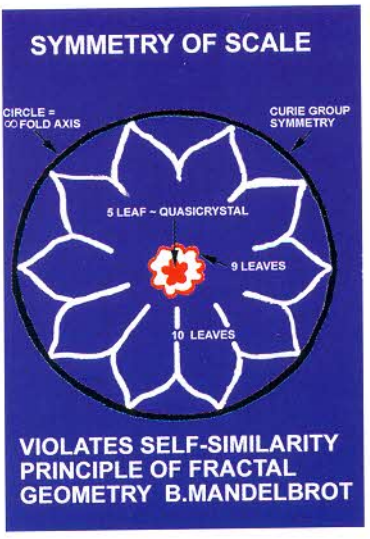

FIGURE 2c - Size effects.

FIGURE 2d - Aperiodicity.

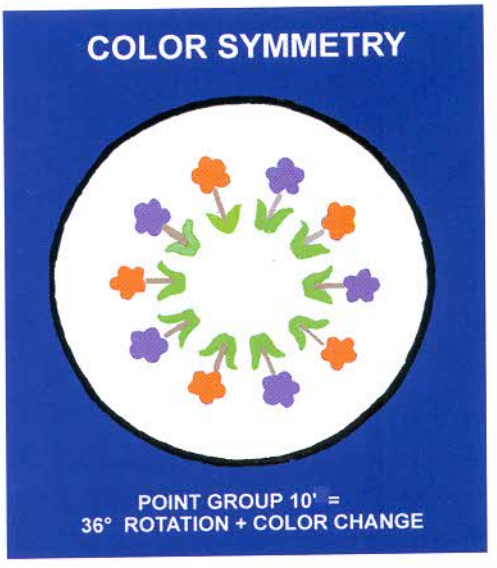

FIGURE 2e - Color patterns.

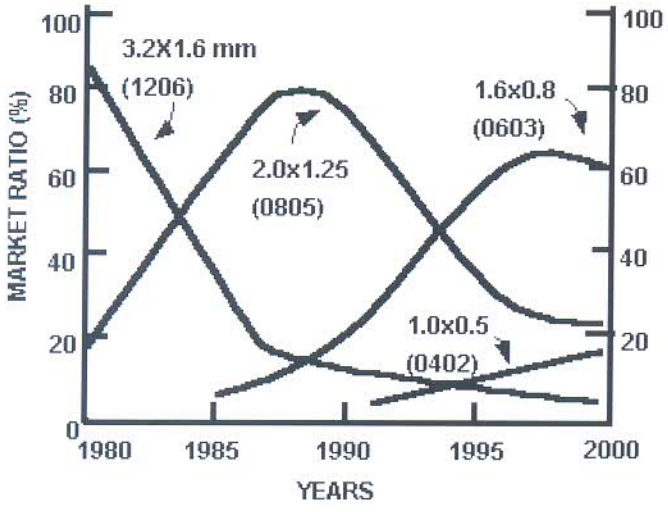

FIGURE 3 - The sizes of ceramic capacitors have decreased steadily with time while the market continues to grow exponentially following Moore's Law.

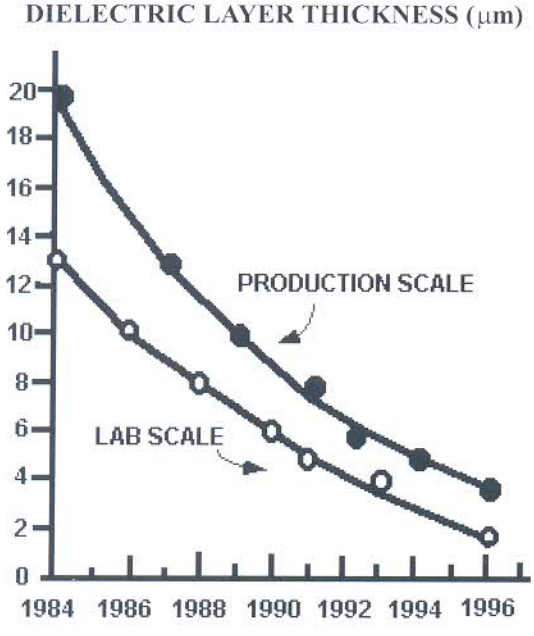

FIGURE 4 - Layer thicknesses in multilayer capacitors are now nearing one micron with grain sizes around 0.2 μm.

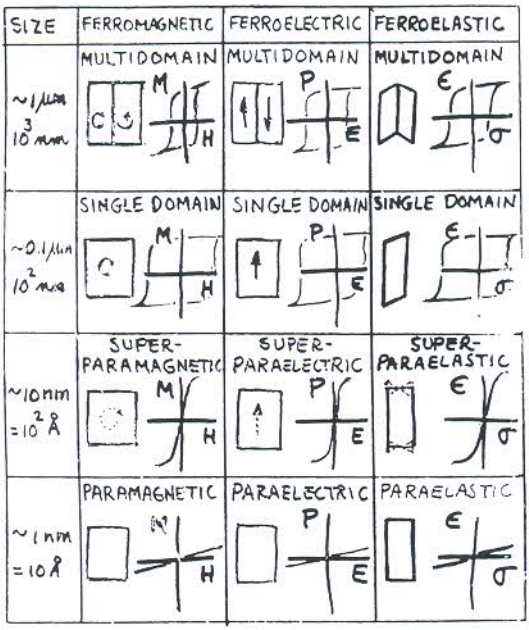

FIGURE 5 - Profound changes in properties take place in ferroic ceramics when the grain sizes drop below the micron range.

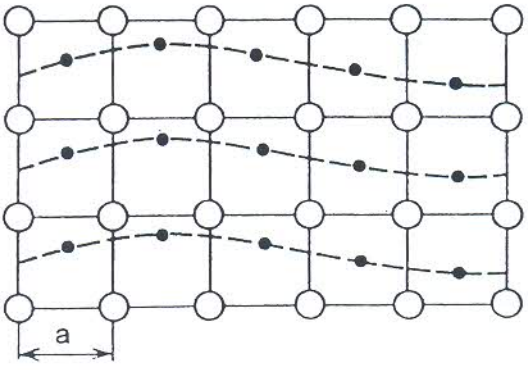

FIGURE 6 - Formation of incommensurate phase as a result of the "freezing" of a displacement wave with a length incommensurate with the unit-cell parameter.

TABLE 1 - Nine types of ferroics in which domain walls can be moved by magnetic fields, electric fields, or mechanical stress. Each is controlled by a different term in the free energy function with an antisymmetry operator relating domain state orientations.

Type	Domain Difference	Antisymmetry Tensor
Primary Ferroics		
Ferromagnetic	Magnetization	Axial First Rank
Ferroelectric	Polarization	Polar First Rank
Ferroelastic	Strain	Polar Second Rank
Secondary Ferroics		
Ferrobielectric	Permittivity	Polar Second Rank
Ferrobimagnetic	Permeability	Polar Second Rank
Ferrobielastic	Elasticity	Polar Fourth Rank
Ferroelastoelectric	Piezoelectricity	Polar Third Rank
Ferromagnetoelectric	Magnetoelectricity	Axial Second Rank
Ferromagnetoelastic	Piezomagnetism	Axial Third Rank

application.

Knowing the optimum symmetry groups, how does one go about creating these symmetries in a real material? Here one applies Curie's Principle of Symmetry Superposition and examines various composite ferroics (Newnham and Giniewicz, 2000). Symmetry patterns can be generated at many different size scales ranging from electron spin arrangements, crystal structures, defect structures, textured grains, tailored domain patterns, electrode geometries, connectivity patterns, and various morphologies using processing methods such as extrusion, tape-casting, and photolithography. Many of the more unusual point groups can be accessed when ferroic materials are prepared as fibers, films, tubes, disks, multilayers and hollow spheres. Using Curie's Principle of Symmetry Superposition, many unusual cross-coupled properties can be optimized by symmetry control. The new feature we are developing is a family of antisymmetry operators (polar vector reversal, polar second rank tensor reversal, axial second rank tensor reversal, etc.) which will augment our understanding of the symmetry of solids, and enable us to predict new families of functional materials for biomedical and industrial applications. Our goal is to control the acoustic and electromagnetic resonance phenomena in a wide range of electroceramic products.

ANTISYMMETRIC CURIE GROUPS

In this section we describe a family of small electroceramic transducers, sensors, and actuators based on black-and-white Curie group symmetries (Fig. 7). One of the goals of this investigation is to control the acoustic vibration modes and radiation patterns by controlling the symmetries of the transducer's material, its external shape and poling pattern, together with the driving electrode geometry. Later we intend to extend these symmetry arguments to electromagnetic wave modes as in millimeter wave resonators and dielectric antennae.

We begin with an example to illustrate the basic idea. Consider a spherical shell made of a piezoelectric ceramic such as PZT with randomly oriented grains. When statistically averaged, randomly oriented grains in an unpoled ceramic conform to spherical symmetry $\infty\infty m1'$ where $\infty\infty$ represents an infinite number of infinite-fold rotation axes, m is an infinite number of mirror planes, and 1′ is the color reversal operator changing white to black, and vice versa.

In ferroelectric substances such as PZT we can use color to represent polar vector reversal. When electrically poled in a strong DC field near T_c, the altered domain structure changes the symmetry to $\infty/m'm$, the symmetry of an electric field. This is also the overall symmetry of an electric dipole with its positive and negatively-charged ends. The ∞-fold axis is parallel to the dipole.

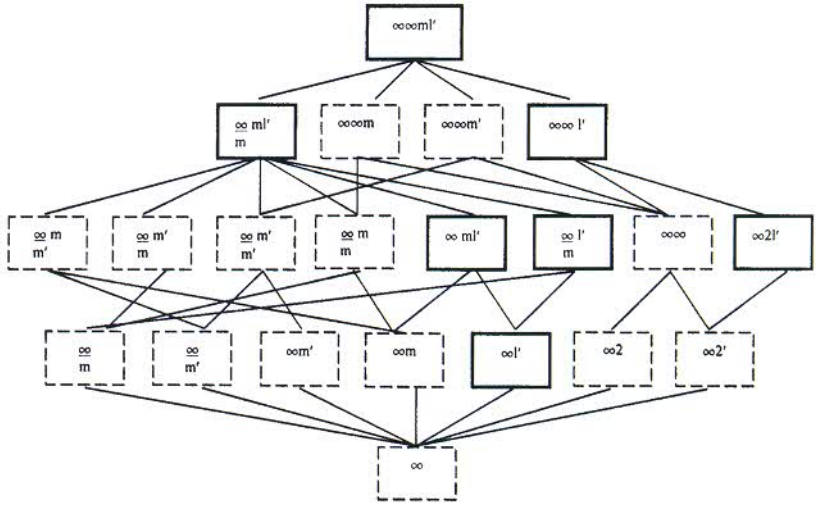

FIGURE 7 - The seven Curie groups (solid boxes) and fourteen black and white Curie groups (dashed boxes). The interconnecting lines denote group-subgroup relationships.

m' is a mirror plane accompanied by charge (color) reversal perpendicular to the ∞-fold axis. In the symbol ∞/m'm, m refers to the infinite number of mirror planes parallel to the ∞-fold dipole axis. This is the symmetry of the material, and that in turn determines the physical properties through Neumann's Law from crystal physics. That of course is why poled PZT is piezoelectric and pyroelectric.

But that is not the only symmetry that is important in transducer design. The vibration modes and radiation patterns depend on the symmetry of the transducer's shape, poling pattern, and driving electrodes as well. If we consider a spherical shell as an example, the shape conforms to spherical symmetry ∞∞m1', and if it is poled radially, the symmetry group changes to ∞∞m. This is a black- and- white symmetry group which exists in two physically-distinct states corresponding to a hollow sphere poled inside-out or outside-in. The principal piezoelectric and pyroelectric coefficients differ in sign for the two states which are related to one another by the symmetry element m¢, reflection accompanied by dipole reversal.

The symmetry of the radially-poled sphere (∞∞m) together with the symmetry of the material (∞/m'm) determines the vibration modes of the transducer. The material symmetry determines the non-zero piezoelectric coefficients: d_{33}, $d_{31} = d_{32}$, $d_{24} = d_{15}$. For a radially-poled sphere, the poling direction X_3 and the driving field E_3 are in the radial direction r, while X_1, and X_2 are orthogonal tangential directions designated by the symbol t. Therefore $d_{33} = d_{rr}$ and $d_{31} = d_{32} = d_{rt}$. When driven electrically, the radially-poled sphere vibrates in two fundamental modes: a high-frequency wall thickness mode governed by d_{rr} and a low-frequency breathing mode controlled by d_{rt}. For a hollow sphere 2 mm in diameter with a wall thickness of about 0.1 mm, these resonances occur near 20 MHz and 600 kHz, respectively (Alkoy, 1999). As discussed later, a much more complex mode spectrum with ellipsoidal modes (symmetry group ∞/mm) is observed when the sphere is electroded at the N and S poles and poled tangentially.

Three additional types of symmetry control can also be illustrated with this example. The first involves re-electroding. The driving electrode pattern need not be the same as the poling electrode pattern. Poling is generally carried out at elevated temperatures under high voltage. After cooling and aging the poling pattern is relatively stable. The poling electrodes can then be removed and a new set of driving electrodes installed which create different vibration modes. This is indicated schematically in Fig. 8. In this way a radially poled sphere might be driven tangentially.

The second modification involves the use of a second transducer attached to the first transducer and driven in a different mode. It is relatively easy to build transducers in multilayer form with a common ground electrode and

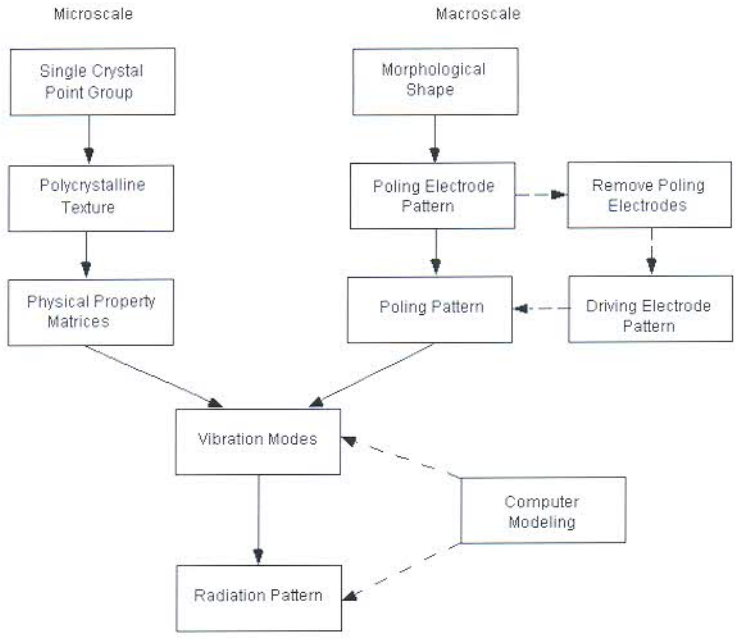

FIGURE 8 - Outline of experimental approach.

independently-driven external electrodes. This enables us to superimpose two vibration modes driven with different phases and amplitudes.

The practical aim of our program is to control the external radiation pattern by controlling the symmetry. If one transducer is driven in an omni-directional fundamental, and the second transducer in a dipole mode, the net result is a cardioid mode. In this way one can direct the radiation in the desired direction.

All of these patterns and their symmetries can be controlled independently by choosing the material and its processing. Our current objective in this research is to access the black-and-white symmetries in Fig.7 to generate interesting acoustic vibration modes using piezoelectric and magnetostrictive transducers.

FERROIC SPHERES, HEMISPHERES, AND RINGS

Our initial aim is to study the vibration modes and radiation patterns from the fourteen black-and-white Curie groups $\infty\infty$m, $\infty\infty$m′, $\infty\infty$, ∞/m′m, ∞/mm′, ∞/m′m′, ∞/mm, ∞/m, ∞/m′, ∞2, ∞2′, ∞m′, ∞m, and ∞. All fourteen symmetries can be accessed with ferroic hollow spheres or modified hollow

spheres shaped as rings or hemispheres. When polished down on one side, hollow spheres (symmetry group ∞∞m1′) become hollow hemispheres (symmetry group ∞m1′). When polished symmetrically on two opposite sides, hollow spheres become rings (symmetry group ∞/mm1′).

Following the processing steps laid out in the experimental procedure section, polycrystalline hollow spheres are prepared from strongly piezoelectric and magnetostrictive substances such as $PbZr_{1-x}Ti_xO_3$ (PZT) and $Tb_{1-x}Dy_xFe_2$ (Terfenol-D). After poling, magnetizing, and polishing all 14 of the black-and-white Curie groups can be generated according to the game plan shown in Table 2.

TABLE 2 - Fourteen black-and-white symmetry groups to be obtained from processed hollow spheres. Initially we are concentrating on the piezoelectric elements, and then the magnetostrictive transducers. Combined elements are to be examined in the third stage using multilayer processing.

Antisymmetric Curie Group	Ferroic Morphology
∞∞m	Radially-poled piezoelectric sphere
∞∞m′	Radially-magnetized magnetostrictive sphere
∞∞∞	Concentric radially-poled piezoelectric sphere and radially-magnetized magnetostrictive sphere
∞/mm	Radially-poled piezoelectric ring
∞/mm′	Longitudinally-magnetized magnetostrictive ring
∞/m′m	Longitudinally-poled piezoelectric ring
∞/m′m′	Radially-magnetized magnetostrictive ring
∞/m	Concentric radially-poled piezoelectric and longitudinally-magnetized magnetostrictive rings
∞/m′	Concentric longitudinally-poled piezoelectric and radially-magnetized magnetostrictive rings
∞2	Concentric radially-poled piezoelectric and radially-magnetized magnetostrictive rings
∞2′	Concentric longitudinally-poled piezoelectric ring and longitudinally-magnetized magnetostrictive ring
∞m	Radially-poled piezoelectric hemisphere
∞m′	Radially-magnetized magnetostrictive hemisphere
∞	Concentric radially-poled piezoelectric and radially-magnetized magnetostrictive hemisphere

The next step is to determine the resonant vibration modes experimentally using impedance spectroscopy and to verify the measurements theoretically using the ATILA finite element code. Typical calculated spectra for a radially-poled piezoelectric hollow sphere and a tangentially poled hollow sphere are illustrated in Figures 9 and 10. For the radially-poled sphere, the low-frequency mode near 600 kHz is a breathing mode driven by piezoelectric coefficient d_{31}, and the high-frequency 20 MHz wall-thickness mode is governed by d_{33}. Miniature hydrophones and minipumps make use of the large hydrostatic piezoelectric coefficient d_h of these transducers. Hollow sphere sensors and actuators have a stress amplification factor proportional to the sphere radius divided by the wall thickness, which is typically more than an order of magnitude in our transducers.

Similar amplification factors apply to the tangentially poled sphere in Fig. 10. This nicely illustrates how to control the vibration modes and their symmetry with the electrode pattern. In this case different size circular electrodes were applied to the top and bottom of the sphere, conforming to antisymmetry group ∞/m'm. When driven electrically, a series of ellipsoidal and egg-shaped vibrations were excited, as illustrated in Figure 10. The ATILA code is very helpful in identifying and visualizing the various modes of vibration of complex patterns and shapes.

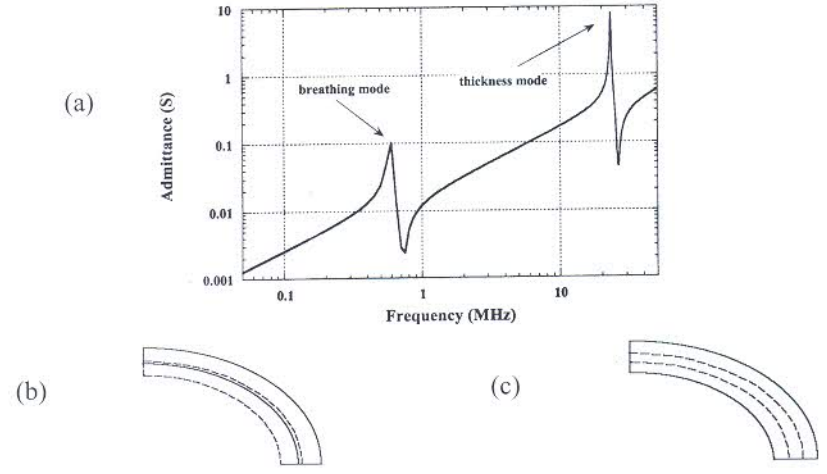

FIGURE 9 - The (a) admittance spectrum of a hollow sphere electroded inside and outside and poled radially. The principal vibration modes are the (b) low frequency breathing mode and the (c) high frequency wall thickness mode. Both modes are spherically symmetric conforming to the shape and electrode pattern. The dashed lines correspond to the rest position and the solid line to the vibration motion. Scales are arbitrary. (Alkoy, 1999)

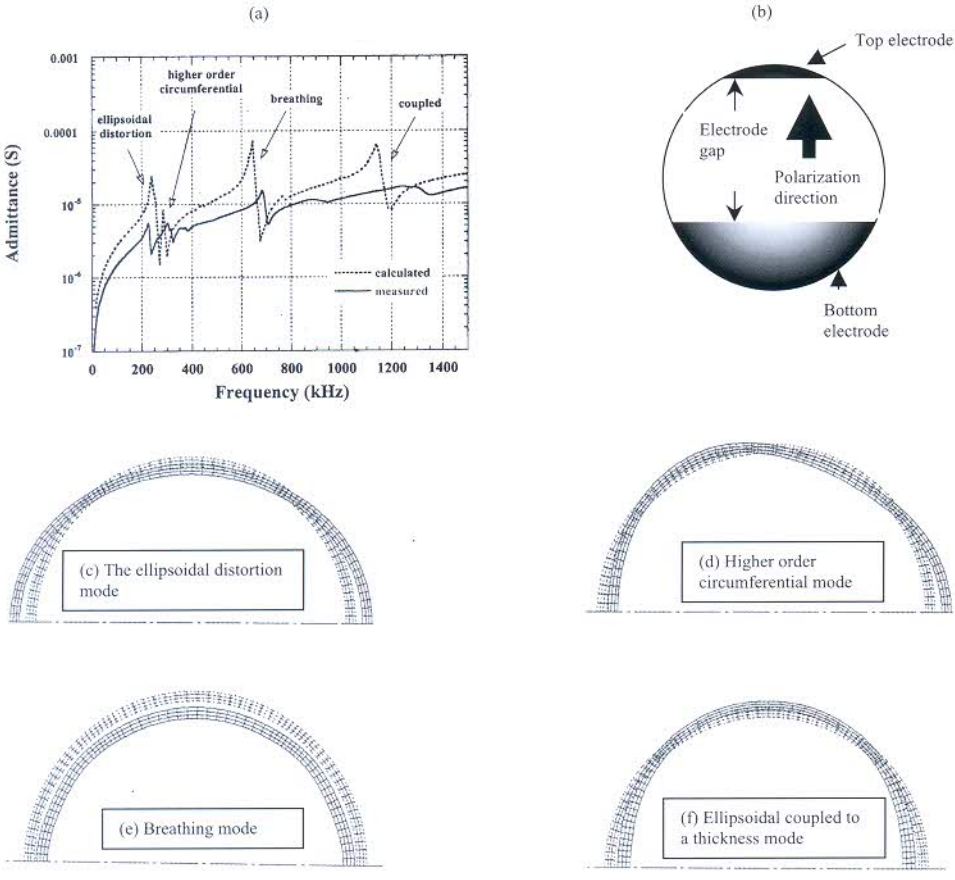

FIGURE 10 - Comparison of the (a) calculated and measured admittance response of (b) a tangentially-poled hollow sphere with asymmetric electrodes. The displacement fields of four vibration modes, two of which are ellipsoidal in shape (∞/mm'), one is spherical (∞∞m'), and one egg-shaped (∞m'). This illustrates Neumann's Principle which says that the symmetry of a property must include the symmetry of the material and the way in which it is driven (Alkoy, 1999).

TRANSDUCER FABRICATION

The fabrication process is designed to produce spherical electroceramic devices with cofired inner electrodes. For commercial applications we need a process capable of producing large quantities of hollow sphere transducers in sizes ranging from a fraction of a millimeter to several millimeters. The process is illustrated schematically in Fig. 11.

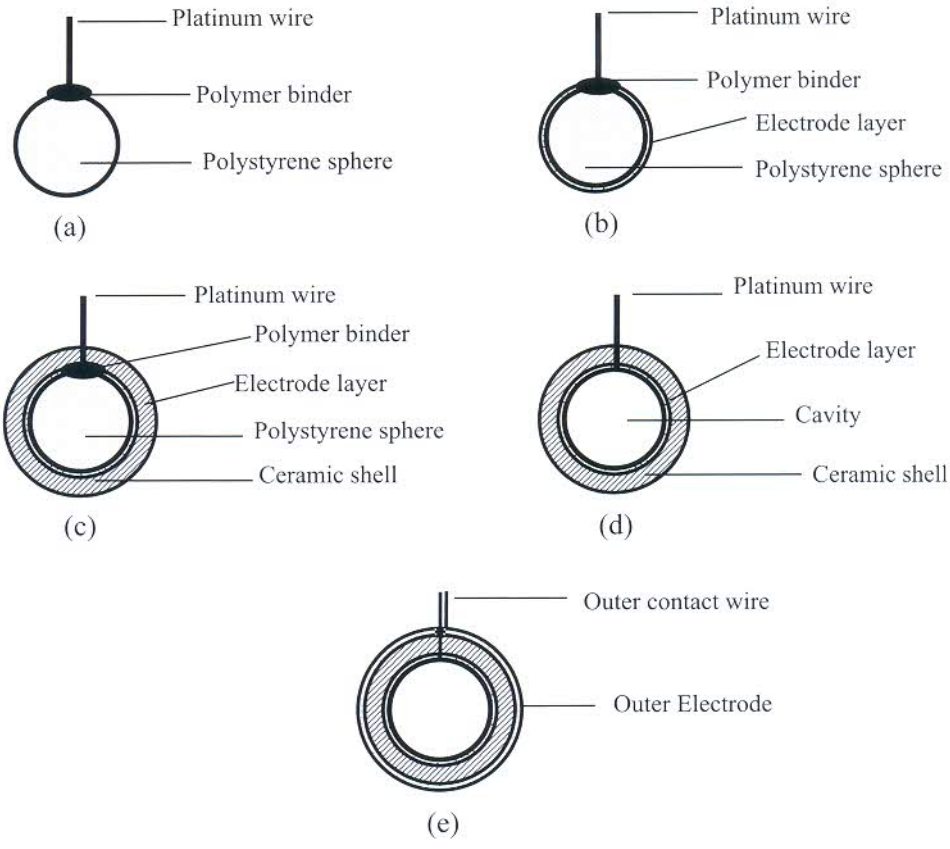

FIGURE 11 - (a) A cross sectional view of the polystyrene spheres with platinum wires attached. A pyrolyzable binder (PVA, etc) is used to keep the wire in position, (b) illustrates the pre-wired polystyrene spheres coated with platinum contained slurry, (c) shows the pre-wired polystyrene spheres coated with a ceramic layer on top of a platinum layer, (d) shows the sintered ceramic hollow sphere with co-fired inner electrode and protruded platinum wire, (e) is a cross sectional view of illustrating the finished spherical transducer by electroding the outer surface of the hollow sphere whose inner surface is already electroded by co-firing.

Thermally decomposable spheres made of polystyrene or hollow polystyrene spheres are used as a fugitive pattern. To achieve a ceramic layer with high green density, a sphere or hollow sphere with a porous structure is preferable. A thin metal wire, typically Pt or Ni, is first attached to the sphere and secured in position using a thermally decomposable binder such as PVA. The wire is used later to apply voltage to the inner electrode. An electrode layer is then coated on the outer surface of the polymer core by dipping it into

a slurry containing metal powders. The electrode is then dried and further serves as a mold for the ceramic slurry. A ceramic shell is then deposited on top of the dried electrode by dipping into a well dispersed ceramic slurry containing binder and dispersant. The ceramic slurry can be aqueous or non-aqueous. The ceramic layer thickness is controlled by immersion time, the solid loading of the ceramic slurry, and its viscosity. When a large wall thickness is desired, multiple coatings can be performed. When the sphere is removed from the slurry, excess slurry on the sphere can be removed by spinning the sphere. Spinning also improves the uniformity of the wall thickness. The porous polystyrene spheres and the electrode layer absorb water from the ceramic layer. The capillary suction allows a dense green body of ceramic shell to be formed, which is crucial in sintering a fully densified ceramic body.

After forming, the spheres are dried and taken through a polymer burnout process in the temperature range between 300 and 700 °C. A ceramic shell with an inner electrode is obtained after this process. Then the ceramic shell is cofired with its electrode. The sintering conditions vary according to the ceramic composition. In most cases, the ceramic and electrode materials are sintered in the temperature range between 1200 and 1400 °C. The immersion time and optimum sintering temperature must be adjusted experimentally to achieve the maximum sintering density of ceramic. For lead containing compositions, the ceramic shell needs to be fired in a closed container in a lead rich atmosphere to reduce lead loss from the ceramic body.

After sintering, the outer surface of the shell is coated with electrode metal through sputtering or dipping. A tiny lead wire is then attached to the outer electrode. The ceramic shell is poled in the case of piezoelectric materials by subjecting the ceramic shell to high electric field at elevated temperatures in the range between 100 and 200 °C. This completes the process of fabricating a hollow spherical transducer.

Multilayer hollow sphere transducers (Fig. 12) can be fabricated by a multiple dipping process to give a structure with alternating electrode and ferroic ceramic layers. After the first ceramic layer is deposited, it is dried and then coated with another layer of electrode material, followed by a coating of another layer of ceramic. Care must be taken to make certain the second electrode layer does not touch the platinum wire and a hole must be left in the second ceramic layer for electrical connection. The goal is to make multilayer hollow spheres with many thin layers similar to multilayer capacitors and multilayer actuators.

After polymer burnout and sintering, the electrodes are connected to electrical lead wires. Different connections are available depending on applications. For receive applications, the layers can be connected in series to improve the receive response. For projector applications, the layers can be

FIGURE 12 - A multilayer hollow spherical transducer prepared using a multiple coating process.

connected in parallel to increase the pressure output to transmit directional beams with the electrodes driven with different phases and amplitudes.

To access certain of the antisymmetric Curie group symmetries (Table 2) it is necessary to convert the hollow spheres into hemispheres or rings. This step is carried out by mounting the hollow sphere in a polymer matrix and polishing the sphere down on one side (for the hemisphere) or two sides (for the ring). The polymer matrix provides the mechanical strength required for the lapping operation.

Limited re-electroding can be accomplished after removing the outer electrodes used in poling the transducer. This enables us to apply driving fields in directions other than the poling field directions, and thereby generate different symmetries and different vibration modes.

ACOUSTIC APPLICATIONS

Applications are not the main focus of this discussion but it is important to have practical goals in mind to justify the research. The increasing use of ultrasonic techniques in biomedical and underwater applications and the sophistication of these techniques has increased the need to characterize the acoustic fields using ultrasonic transducers. In the last forty years several different techniques and probe designs have been employed for this purpose, including rod-guided waves, thermoacoustic sensors, fiberoptic sensors utilizing acousto-optic interaction, and miniature acoustic probes made from ceramic and polymer-based piezoelectrics. Miniature ultrasonic probes have been used both for mapping the field of a hydrophone as well as the nonacoustic field of turbulent flow. There are, however, several important requirements for micro-probe sensors in these applications. In detecting underwater signals or biological pressure waves, omnidirectionality is highly advantageous. Accurate mapping of an acoustic field requires that: (i) the physical dimensions of the probe

should be smaller than the acoustical wavelength of interest, (ii) the resonance frequencies of the probe should be well above the frequency range of interest, (iii) adequate sensitivity with an acceptable signal-to-noise ratio and (iv) wide bandwidth.

Although volume expanders with spherical shape are thought to be the best way to achieve omnidirectionality, there are problems associated with fabricating hollow spheres with sizes in the millimeter range, as pointed out by previous researchers. There are a number of examples of transducers prepared from piezoelectric plates, but these transducers have a pronounced directivity even when the probe dimensions are smaller than a wavelength. Solutions proposed previously for the directivity problem include solid-core spherical probes and hollow cyclindrical probes.

In addition to the underwater applications, spherically shaped transducers are also desirable in medical ultrasound applications. Examples include a quasi-omnidirectional polymer-based transducer developed for ultrasonic guidance of intravascular catheters and a focused transducer for biomedical ultrasonic imaging, prepared from a spherical ceramic shell. Every year millions of medical procedures are performed in the United States using catheter systems a few millimeters in diameter. Typically, they are inserted through the skin into blood vessels or into various body cavities to deliver drugs or therapeutic devices.

At present catheters are guided with real-time X-ray imaging (fluoroscopy) despite the advantages of ultrasound imaging over X-ray imaging in terms of cost, safety and availability. Because the wavelengths used in medical ultrasonic imaging (0.2-0.5 mm) are several times smaller than the catheter, it acts as a reflector and the ultrasonic visibility of the catheter is highly direction dependent with regard to external ultrasonic beams. One solution to this problem is to mount an omnidirectional ultrasonic transducer on the catheter that can serve as an ultrasonic marker to help locate the catheter without the use of hazardous X-rays. The applications of these ultrasonic imaging catheters include guiding balloon angioplasties of the leg, guiding catheters inside the heart to ablate incorrectly functioning cardiac tissue, and guiding catheters within the uterus to inject fluid into the fallopian tubes to test for tubal blockage. Ceramic hollow sphere transducers have the required omnidirectionality and high sensitivity and can be electrically matched to the electronic systems.

It is our hope that the miniature hollow sphere transducers described in this paper will help satisfy the size, directionality and acoustic impedance matching requirements for biomedical and underwater applications. Later we hope to manufacture the transducers in large numbers by a simple inexpensive process, which makes it possible to mass-produce throw-away transducers. The basic understanding of vibration modes in small spherical transducers provided by this symmetry-guided approach will help immensely.

REFERENCES

1. S. Alkoy, *Piezoelectric Hollow Sphere Transducers*, Penn State University Ph.D. Thesis in Materials Science and Engineering, p. 89 and p. 111 (1999).
2. R.R. Birss, *Symmetry and Magnetism*, North-Holland Publishing Co., Amsterdam (1964).
3. R.E. Newnham, *Domains in Minerals*, **Amer. Mineralogist**, Vol. 59, p. 906-918 (1974).
4. R.E. Newnham and L.E. Cross, *Symmetry of Secondary Ferroics*, **Mat. Res. Bull.**, Vol. 9, p. 927-934 and 1021-1032 (1974).
5. R.E. Newnham and J.R. Giniewicz, *Nonmechanical Properties of Composites*, **Comprehensive Materials**, Vol. 1, p. 431-463 (2000).
6. W. Voigt, *Lehrbuch der Kristallphysik*, B.G. Teubner, Leipzig (1928).